Simultaneous triple-modality imaging of diffuse reflectance, optoacoustic pressure and ultrasonic scattering using an acoustic-resolution photoacoustic microscope: feasibility study

2016 Laser Phys. Lett. 13 025605

(http://iopscience.iop.org/1612-202X/13/2/025605)

IOP Publishing | Astro Ltd
Laser Physics Letters
Laser Phys. Lett. 13 (2016) 025605 (7pp)
doi:10.1088/1612-2011/13/2/025605

Simultaneous triple-modality imaging of diffuse reflectance, optoacoustic pressure and ultrasonic scattering using an acoustic-resolution photoacoustic microscope: feasibility study

Pavel Subochev[1], Ilya Fiks[1], Martin Frenz[2] and Ilya Turchin[1]

[1] Institute of Applied Physics RAS, 46 Ulyanov Street, Nizhny Novgorod 603950, Russia
[2] University of Bern, Institute of Applied Physics, 5 Sidlerstrasse, Bern, CH-3012, Switzerland

E-mail: Pavel.Subochev@gmail.com

Received 24 November 2015
Accepted for publication 2 December 2015
Published 7 January 2016

Abstract

The letter discusses the opportunity for cost-effective use of conventional optoacoustic hardware to realize additional imaging modalities such as ultrasonic microscopy and diffuse optical reflectometry within the same laser pulse. Optoacoustic methods for deep biomedical visualization are based on pulsed laser illumination of the internal tissue layers with scattered photons, however some of the back-scattered photons can be absorbed by the optoacoustic detector. Thermoelastic extension of the detector's surface provides a probing pulse for an ultrasonic modality while the measurement of the amplitude of the probing ultrasonic pulse allows estimation of the diffuse reflectance from the object under investigation.

Keywords: photoacoustic microscopy, ultrasonic microscopy, diffuse optical reflectometry

(Some figures may appear in colour only in the online journal)

1. Introduction

Optoacoustic (OA) (or photoacoustic) imaging is a modern method of biomedical visualization based on the remote detection of ultrasonic (US) waves generated in the tissue under investigation due to the local absorption of nanosecond laser pulses by optical heterogeneities [1]. Hybrid methods of OA imaging [2] combine the advantages of both the optical [3] and US modalities [4]. The large differences in the optical absorption by the target endogenous [5, 6] or exogenous [7, 8] chromophores ensure that the OA images have a high contrast-to-noise ratio, while the minimal US scattering [9] and frequency-dependent US attenuation [10] of biotissues determine the scalable diagnostic depth and spatial resolution [11–14].

Modern clinical facilities demand [15] multi-spectral OA imaging systems that are capable of 3D reconstruction of tissue chromophore concentrations [16]. However, leading optoacoustic groups have highlighted the multiple challenges [17, 18] facing quantitative optoacoustic imaging (QOI). One of the most significant aspects of QOI is the unknown spatial distribution of the optical fluence inside the biological tissue that impacts on the amplitudes of the OA pressure signals being generated [19, 20]. For independent measurements of optical fluence, some authors [21–28] have proposed utilizing additional methods, such as diffuse optical tomography, alongside the traditional OA systems. However, due to the limited space above the object being imaged [29] the incorporation of independent diffuse optical equipment into the OA imaging head can be challenging, especially in the case of reflection-mode geometries.

Consider the peculiarities of optical fluence distribution [30] within typical background biological tissue characterized by its lower optical absorbtion coefficient compared to the

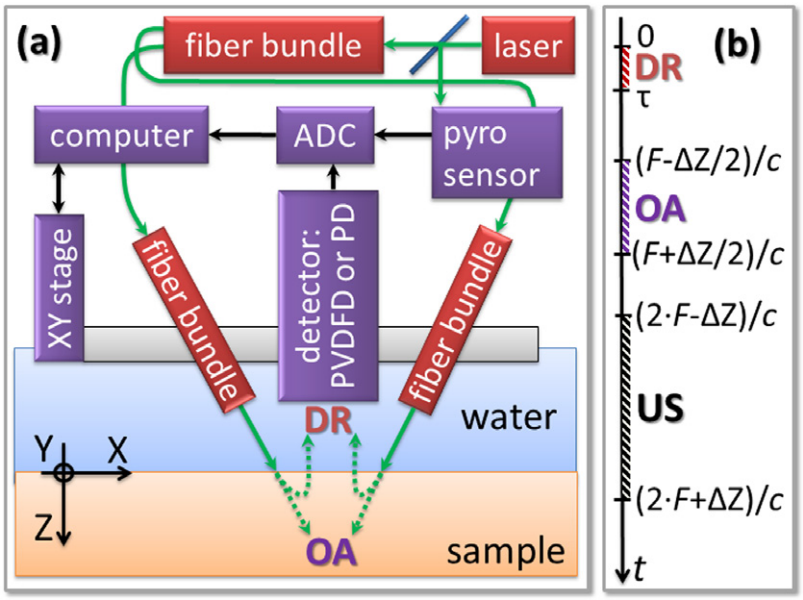

Figure 1. The experimental setup for OA/US/DR imaging. (a) Schematic of the experimental setup: photons absorbed by the sample generate OA signals, while photons absorbed by OA detector generate the measurable DR signal as well as providing the probing US pulse. (b) Sketch of the information contained in an A-scan with the sequence of the DR, OA, and US signals.

reduced scattering coefficient [31]. While strong heterogeneities of optical absorption (e.g. caused by blood vessels) are rarely distributed over the background tissue, some incident photons may not deposit their energy at the absorbing heterogeneities within the investigated object but may be scattered back through the surface of the sample. These back-scattered photons can be absorbed by the surface of the optoacoustic detector, providing a cost-effective means of generating a probing US pulse. The benefits of a transition from a single-modality acoustical-resolution OA system [32, 33] to dual-modality OA/US imaging using the backscattered light has been discussed in [34, 35].

In this feasibility study we kept the functionality of the previously-reported dual-modality system, but we additionally measured the signals from the back-scattered photons captured by the surface of the optoacoustic detector. The main challenge was to keep the diffuse reflectance (DR) signal within the dynamic range of the conventional dual-modality hardware as set up to measure the OA and US signals. We should note, that the DR does not directly quantify the optical fluence distribution within the illuminated sample, but it can be used to provide additional information for solving QOI inverse problems [36–41]. However, this letter is not intended to discuss the application of diffuse optical reflectometry to QOI.

2. Materials and methods

In figure 1(a) we present the experimental setup for triple-modality imaging based on our previously developed dual-modality OA/US microscope. A solid-state laser, LT-2214-PC (LOTIS TII, Belorussia), provides $\tau = 18$ ns optical pulses across a tunable 400–2100 nm wavelength range with a 10 Hz pulse repetition rate. The output laser beam is collimated into a fiber bundle (Ceram Optec, Germany). The fourteen output arms of the fiber bundle (each arm of 2.5 mm diameter and with a 0.17 numerical aperture in water) are homogeneously distributed along a conical surface at an angle of 40 degrees [42] to the Z axis to provide illumination of the sample. A custom-made 10:90 beam splitter with a calibrated pyroelectric sensor ES111C (Thorlabs, USA) is used to determine the energy for each single laser pulse at the distal fiber tips. This measurement is needed both to normalize the OA images and to calculate the effective radiant exposure at the surface of the sample. The radiant exposure is kept below 10 mJ cm^{-2} to satisfy the 20 mJ cm^{-2} ANSI Z136.1 standard for laser safety.

A polyvinylidene difluoride detector (PVDFD) PI-35-2 (Olympus-NDT, USA) with NA = 0.25, $f = 32$ MHz central frequency, $\Delta f = 34$ MHz frequency band and $F = 12.7$ mm spherical focus is directed into the center of the area of optical illumination [43]. The analog signals from the PVDFD are sent to an analog-to-digital converter (ADC) based on an NI5761 14-bit 250-MS/s adapter with an NI FlexRIO FPGA PXI-7952R module (National Instruments, USA).

The scanning head (figure 1(a)) is mounted on two linear positioning slides (Automation Gages, USA), with a maximum travel range of 6.25 mm, driven by AM-23-239-3 step motors (Advance Microsystems, USA), inside an immersion chamber filled with distilled water. The movement of the translation stage is matched to the 10 Hz repetition rate of the laser pulses. Polyethylene foil of thickness 60 μm covers the bottom of an immersion chamber separating the water and the sample.

To realize triple-modality DR/OA/US imaging the automation algorithm inquires the scanning range $\Delta X = \Delta Z$, the scanning step size δx, the focal length F, the average speed of sound c in the medium, and the effective duration of the laser pulse τ. Figure 1(b) schematically represents the sequence of signals to be registered by the PVDFD at each

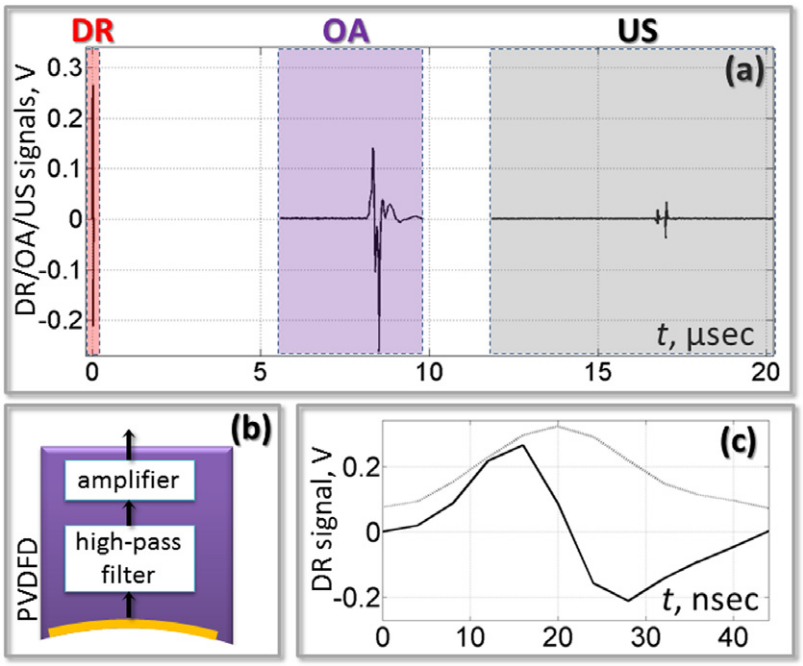

Figure 2. Triple-modality measurements using the OA detector. (a) Sample A-scan with DR/OA/US signals. (b) Spherically-focused PVDFD used for the measurements. (c) Band-limited sample DR signal (solid line) and its envelope (dotted line).

of the $\Delta X/\delta x$ scanning positions of the optoacoustic head as a result of illumination of the sample by each single laser pulse. The DR signal is detected during the time period from $t = 0$ (corresponding to the beginning of the laser pulse) to $t = 2\tau$. The OA A-scan is detected during the time period from $t = (F - \Delta Z/2)$/c to $t = (F + \Delta Z/2)/c$. The US A-scan is detected during the time period from $t = (2F - \Delta Z)/c$ to $t = (2F + \Delta Z)/c$.

The sample A-scan containing the DR/OA/US signals is presented in figure 2(a). Note that the PVDFD contains a built-in custom-made 5 MHz high-pass filter and a custom-made AD4817-based 50 dB amplifier (figure 2(b)). The high-pass filter eliminates any low frequency pyroelectric signals correlating with the OA and US signals and therefore allows the DR/OA/US signals to remain within the 2.07 V peak-to-peak input range of the ADC (figure 2(a)).

Figure 2(c) represents the sample DR signal and its envelope (obtained using Hilbert's transform) corresponding to the backscattered light absorbed by the surface of the PVDFD. Filtered DR signal has an N-shaped form, while its envelope is close to a Gaussian form with an 20 ns effective duration exceeding the 4 ns sampling period of the ADC. We define the signal-to-noise ratio (SNR) for the DR modality as the ratio between the envelope of the DR signal integrated over the effective 20 ns laser pulse duration, and the standard deviation of the noise.

To validate the results of the DR measurements with the PVDFD we also provided the facility for replacing the PVDFD with a DET10A (Thorlabs, USA) photodetector (PD) [44, 45]. The backscattered photons were transferred to the PD using a custom-made fiber bundle with a 6.5 mm aperture (similar to the aperture of the PVDFD) through an NE20A (Thorlabs, USA) absorptive neutral density filter. No optical lens was used between the object and the fiber bundle.The signals from the PD were digitized using the same ADC and were also integrated over the 20 ns effective laser pulse duration.

3. Results and discussion

Figure 3 presents the DR SNRs measured from three 60 mm × 15 mm petri dishes containing 0%, 0.15%, and 1.5% aqueous solutions of lipofundin (B. Braun Melsungen AG, Germany) as diffusive reference standards for the tissue simulating phantoms [46]. To minimize possible reflections, the bottoms of the petri dishes were covered with black oracal tape (Orafol, Germany). Each petri dish was scanned within the $\Delta X = 6$ mm scanning range using a $\delta x = 4$ μm scanning step size. A laser wavelength of 532 nm was used; the radiant exposure was tuned in the 0.3–10 mJ cm^{-2} range. When using identical radiant exposures, the greater the concentration of lipofundin, the larger was the number of backscattered photons reaching the PD and the PVDFD.

The three times lower SNR for the PVDFD was caused by the larger standard deviation of the noise due to the amplifier circuit, and the lower 'quantum effeciency' of the PVDFD caused by its highly reflective metallized surface. For the 0.15% concentration of lipofundin the value of the linear regression coefficient: R^2(PVDFD) = 0.996, proves the linearity of the DR technique in the 0.3–10 mJ cm^{-2} range of radiant exposure commonly used for optoacoustic sensing. Random deviations around the linear fit correspond to the speckle noise (4% for the PVDFD and 7% for the PD) typical of coherent light sources. Both detectors provide linear responses across very high dynamic ranges, nevertheless the ADC response is limited, so, for high backreflection of the

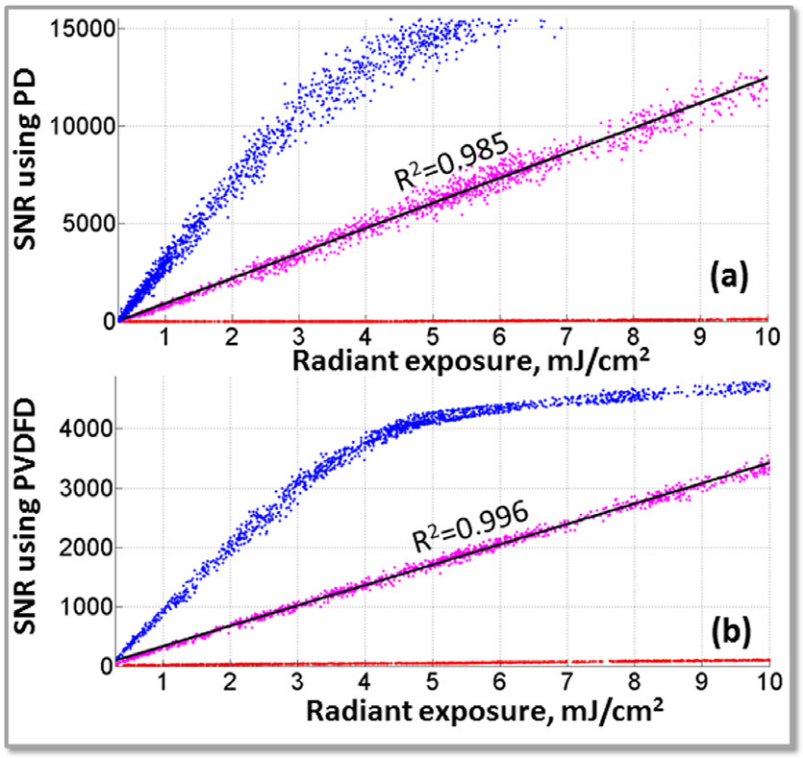

Figure 3. (a), (b) The DR SNRs measured using the PVDFD or PD in three phantoms: (red)—distilled water; (magneta)—0.15% aqueous solution of lipofundin; (blue)—1.5% aqueous solution of lipofundin; (black)—linear fit to experimental data.

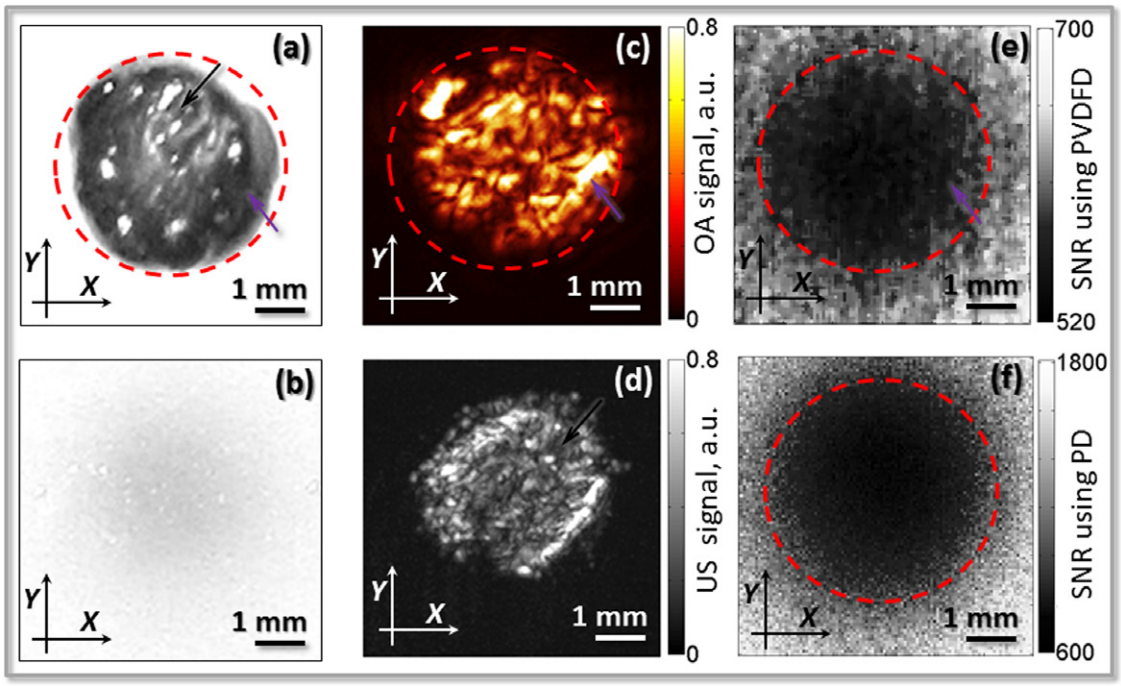

Figure 4. The results of 2D imaging. (a) photograph of black agar droplet; (b) photograph of the phantom containing the agar droplet at 1 mm depth in 0.5% aqueous solution of lipofundin; (c) OA C-scan of the phantom using PVDFD; (d) US C-scan of the phantom using PVDFD; (e) DR image using PVDFD; (f) DR image using PD. Red circles indicate the shape of the agar droplet as the larger-scale heterogeneitiy of optical scattering and absorbtion visualized in the DR images. Magenta arrows indicate one of the smaller-scale heterogeneities of the optical absorbtion visualized in the OA and PVDFD DR image. Black arrow indicates one of the smaller-scale heterogeneities of the acoustic impedance visualized in the US image.

scattering medium (1.5% concentration of lipofundin), some non-linear response can be observed above the thresholds of 3500 and 13 000 for the PVDFD and the PD, respectively.

To investigate the opportunities for simultaneous triple-modality OA/US/DR imaging we manufactured a 2% agar droplet (figure 4(a)) formed from a 4% aqueous solution of black drawing ink (Koh-i-Nor, Czech Republic). The agar droplet was immersed into a 0.5% aqueous solution of lipofundin to a depth of 1 mm (figure 4(b)). This phantom was scanned in the *XY* directions across the $\Delta X = \Delta Y = 6$ mm scanning range, using $\delta x = \delta y = 60$ μm step size. The PVDFD was focused on the upper surface of the agar droplet. OA and US C-scans corresponding to the focal region of the PVDFD are presented in figures 4(c) and (d). No beam-forming algorithms such as [47–49] were used to improve the lateral resolution. Figure 4(e) represents the DR image formed of the phantom using the PVDFD. The DR image clearly represents a region with a low diffuse reflectance in the center of the phantom, caused by the absorption of backscattered photons by the agar droplet.

After replacing the PVDFD with the PD the *XY* scanning procedure was repeated to obtain a corresponding DR image of the phantom (figure 4(f)). The noise within both DR images could have been further decreased by using advanced despeckle techniques [50]. Nevertheless, only the PVDFD (figure 4(e)) provided the ability to distinguish most of the absorbing heterogeneities within the black agar droplet also seen in the OA image (figure 4(c)). One possible reason is the smaller deviation of the speckle noise characterizing the PVDFD (figure 3(b)). Another, is that the spherical surface of the PVDFD, itself, can work as an optical lens, providing a finite radiation pattern in the DR modality. However, the possibility that the PVDFD introduces its own optical focusing needs to be studied in more detail using other spherically focused PVDFDs with different numerical apertures.

As the amplifier and high-pass filter (figure 2(b)) allowed the DR/OA/US to be kept within the dynamic range of the ADC for this particular sample (figures 4(a) and (b)), use of the PVDFD allowed us obtain OA/US images of the same object (figures 4(c) and (d)) simultaneously with the DR image (figure 4(e)). However, for some highly-scattering biological tissues the amplitude of the DR signal can significantly exceed the OA and US signals. In such cases it would be possible to use a nanosecond switcher with two amplifiers: the amplifier with the smaller gain to be switched to measure the DR signal, and the amplifier with the higher gain to be switched to measure the OA/US signals.

4. Conclusion

We have presented the opportunities for cost-effective triple-modality DR/OA/US imaging using conventional optoacoustic hardware. In our study the DR measurements were based on the detection of a thermoelastic signal generated due to the absorption of backscattered photons by the metalized surface of a PVDFD.

Experiments with homogeneous intralipid phantoms allow us to conclude, that the capabilities of the PVDFD to measure DR compare well with the capabilities of the kind of PD traditionally used for DR measurements. For a 0.15% lipofundin concentration both the PD and PVDFD demonstrated linearity of their DR signals up to radiant exposures of 10 mJ cm^{-2}. However, the PVDFD demonstrated smaller deviations in its speckle noise.

Using an inhomogeneous phantom with the PVDFD we demonstrated the opportunity for keeping the DR/OA/US signals within the dynamic range of the ADC. We also compared the optical focusing of the PD and the PVDFD and concluded that the PVDFD has the potential to provide DR images of non-homogeneous samples with better spatial resolutions. The better quality of the DR image provided by the PVDFD may be caused by the spherical surface of the PVDFD acting like an optical lens. However, the possibility of providing focused optical detection by using a spherically-focused PVDFD requires more detailed investigation.

Generally, the simultaneous DR technique can be realized as a ‘free’ upgrade to other optoacoustic systems, however two important factors need to be taken to account. Highly scattering biological tissues can result in saturation of the DR signal, so it might be important to preset different gains for the DR and OA/US signals. The absorption of backscattered light by the surface of the PVDFD causes a low-frequency pyroelectric signal that needs to be removed using an analog filter to avoid its unwanted contribution to the OA and US signals. Conventional narrowband OA detectors should already be free from unnecesasary low-frequency components, however the shape of the DR signal can be more complicated than the N-shaped pulses detected in our study using a fairly wideband PVDFD.

As the problem of the direct determination of optical fluence within biological tissue remains one of the major challenges in the development of OA methods for clinical use, perhaps the most valuable future application presented by the PVDFD DR technique will be in quantitative optoacoustic imaging. In general, to make optoacoustic quantifications easier, the relationships of the DR signal to the optical fluence and the absorption should be specified within the analytical or Monte-Carlo model. Although the transition from homogeneous bulk phantoms to biological tissues may reveal possible limitations of the DR technique, there is a strong economic case for further investigation of the *in vivo* application of simultaneous DR/OA/US measurements.

Acknowledgments

This work was supported financially by the Russian Science Foundation (project No14-15-00709). The authors are grateful to Roman Belyaev, Vladimir Vorobyev, Sergey Pozhidaev, and Dr A Postnikova for their engineering contributions to this work and to Dr M Kirillin for his valuable discussions.

References

[1] Beard P 2011 Biomedical photoacoustic imaging *Interface Focus*

[2] Niederhauser J J, Jaeger M, Lemor R, Weber P and Frenz M 2005 Combined ultrasound and optoacoustic system for real-time high-contrast vascular imaging *in vivo IEEE Trans. Med. Imaging* **24** 436–40

[3] Ntziachristos V, Yodh A, Schnall M and Chance B 2000 Concurrent MRI and diffuse optical tomography of breast after indocyanine green enhancement *Proc. Natl Acad. Sci.* **97** 2767–72

[4] Bouchard R, Sahin O and Emelianov S 2014 Ultrasound-guided photoacoustic imaging: current state and future development *IEEE Trans. Ultrason. Ferroelectr. Freq. Control* **61** 450–66

[5] Petrov A, Wynne K E, Parsley M A, Petrov I Y, Petrov Y, Ruppert K A, Prough D S, DeWitt D S and Esenaliev R O 2014 Optoacoustic detection of intra-and extracranial hematomas in rats after blast injury *Photoacoustics* **2** 75–80

[6] Grootendorst D, Jose J, Wouters M, van Boven H, Van der Hage J, Van Leeuwen T, Steenbergen W, Manohar S and Ruers T 2012 First experiences of photoacoustic imaging for detection of melanoma metastases in resected human lymph nodes *Lasers Surg. Med.* **44** 541–9

[7] Oraevsky A A 2015 Contrast agents for optoacoustic imaging: design and biomedical applications *Photoacoustics* **3** 1–2

[8] Zhang R, Pan D, Cai X, Yang X, Senpan A, Allen J S, Lanza G M and Wang L V 2015 $\alpha\nu\beta$3-targeted copper nanoparticles incorporating an Sn 2 lipase-labile fumagillin prodrug for photoacoustic neovascular imaging and treatment *Theranostics* **5** 124

[9] Jaeger M, Held G, Peeters S, Preisser S, Grünig M and Frenz M 2015 Computed ultrasound tomography in echo mode for imaging speed of sound using pulse-echo sonography: proof of principle *Ultrasound Med. Biol.* **41** 235–50

[10] Kruger R A, Kuzmiak C M, Lam R B, Reinecke D R, Del Rio S P and Steed D 2013 Dedicated 3D photoacoustic breast imaging *Med. Phys.* **40** 113301

[11] Wang L V and Hu S 2012 Photoacoustic tomography: *in vivo* imaging from organelles to organs *Science* **335** 1458–62

[12] Yang J-M, Favazza C, Chen R, Yao J, Cai X, Maslov K, Zhou Q, Shung K K and Wang L V 2012 Simultaneous functional photoacoustic and ultrasonic endoscopy of internal organs *in vivo Nat. Med.* **18** 1297–302

[13] Estrada H, Turner J, Kneipp M and Razansky D 2014 Real-time optoacoustic brain microscopy with hybrid optical and acoustic resolution *Laser Phys. Lett.* **11** 045601

[14] Hajireza P, Shi W and Zemp R 2013 Label-free *in vivo* GRIN-lens optical resolution photoacoustic micro-endoscopy *Laser Phys. Lett.* **10** 055603

[15] Harrison T J 2014 Clinical transitions in photoacoustic imaging *Department of Electrical and Computer Engineering* (Urbana: Engineering Publications Office) p 182

[16] Kim C, Favazza C and Wang L V 2010 *In vivo* photoacoustic tomography of chemicals: high-resolution functional and molecular optical imaging at new depths *Chem. Rev.* **110** 2756–82

[17] Cox B, Laufer J G, Arridge S R and Beard P C 2012 Quantitative spectroscopic photoacoustic imaging: a review *J. Biomed. Opt.* **17** 0612021–2

[18] Lutzweiler C and Razansky D 2013 Optoacoustic imaging and tomography: reconstruction approaches and outstanding challenges in image performance and quantification *Sensors* **13** 7345–84

[19] Caravaca-Aguirre A M, Conkey D B, Dove J D, Ju H, Murray T W and Piestun R 2013 High contrast three-dimensional photoacoustic imaging through scattering media by localized optical fluence enhancement *Opt. Express* **21** 26671–6

[20] Held G, Preisser S, Akarçay H G, Peeters S, Frenz M and Jaeger M 2014 Effect of irradiation distance on image contrast in epi-optoacoustic imaging of human volunteers *Biomed. Opt. Express* **5** 3765–80

[21] Kumavor P D, Xu C, Aguirre A, Gamelin J, Ardeshirpour Y, Tavakoli B, Zanganeh S, Alqasemi U, Yang Y and Zhu Q 2011 Target detection and quantification using a hybrid hand-held diffuse optical tomography and photoacoustic tomography system *J. Biomed. Opt.* **16** 046010–12

[22] Bauer A Q, Nothdurft R E, Erpelding T N, Wang L V and Culver J P 2011 Quantitative photoacoustic imaging: correcting for heterogeneous light fluence distributions using diffuse optical tomography *J. Biomed. Opt.* **16** 096016–7

[23] Xi L, Li X, Yao L, Grobmyer S and Jiang H 2012 Design and evaluation of a hybrid photoacoustic tomography and diffuse optical tomography system for breast cancer detection *Med. Phys.* **39** 2584–94

[24] Ren K, Gao H and Zhao H 2013 A hybrid reconstruction method for quantitative PAT *SIAM J. Imaging Sci.* **6** 32–55

[25] Xu C, Kumavor P D, Alqasemi U, Li H, Xu Y, Zanganeh S and Zhu Q 2013 Indocyanine green enhanced co-registered diffuse optical tomography and photoacoustic tomography *J. Biomed. Opt.* **18** 126006

[26] Gibson A, Hebden J and Arridge S R 2005 Recent advances in diffuse optical imaging *Phys. Med. Biol.* **50** R1

[27] Daoudi K, Hussain A, Hondebrink E and Steenbergen W 2012 Correcting photoacoustic signals for fluence variations using acousto-optic modulation *Opt. Express* **20** 14117–29

[28] Dai X, Xi L, Duan C, Yang H, Xie H and Jiang H 2015 Miniature probe integrating optical-resolution photoacoustic microscopy, optical coherence tomography, and ultrasound imaging: proof-of-concept *Opt. Lett.* **40** 2921–4

[29] Mallidi S, Luke G P and Emelianov S 2011 Photoacoustic imaging in cancer detection, diagnosis, and treatment guidance *Trends Biotechnol.* **29** 213–21

[30] Jacques S L 2010 How tissue optics affect dosimetry of photodynamic therapy *J. Biomed. Opt.* **15** 051608–6

[31] Jacques S L 2013 Optical properties of biological tissues: a review *Phys. Med. Biol.* **58** R37

[32] Jeon M, Kim J and Kim C 2014 Multiplane spectroscopic whole-body photoacoustic imaging of small animals *in vivo Med. Biol. Eng. Comput.* 1–12

[33] Omar M, Soliman D, Gateau J and Ntziachristos V 2014 Ultrawideband reflection-mode optoacoustic mesoscopy *Opt. Lett.* **39** 3911–4

[34] Subochev P, Katichev A, Morozov A, Orlova A, Kamensky V and Turchin I 2012 Simultaneous photoacoustic and optically mediated ultrasound microscopy: phantom study *Opt. Lett.* **37** 4606–8

[35] Subochev P, Orlova A, Shirmanova M, Postnikova A and Turchin I 2015 Simultaneous photoacoustic and optically mediated ultrasound microscopy: an *in vivo* study *Biomed. Opt. Express* **6** 631–8

[36] Yuan Z and Jiang H 2006 Quantitative photoacoustic tomography: recovery of optical absorption coefficient maps of heterogeneous media *Appl. Phys. Lett.* **88** 231101

[37] Bu S, Liu Z, Shiina T, Kondo K, Yamakawa M, Fukutani K, Someda Y and Asao Y 2012 Model-based reconstruction integrated with fluence compensation for photoacoustic tomography *IEEE Trans. Biomed. Eng.* **59** 1354–63

[38] Saratoon T, Tarvainen T, Cox B and Arridge S 2013 A gradient-based method for quantitative photoacoustic tomography using the radiative transfer equation *Inverse Problems* **29** 075006

[39] Esposito R, Martelli F and De Nicola S 2014 Closed-form solution of the steady-state photon diffusion equation in the presence of absorbing inclusions *Opt. Lett.* **39** 826–9

[40] Shao P, Harrison T J and Zemp R J 2014 Consecutively reconstructing absorption and scattering distributions in turbid media with multiple-illumination photoacoustic tomography *J. Biomed. Opt.* **19** 126009

[41] Yuan Z, Li X and Xi L 2014 Listening to light scattering in turbid media: quantitative optical scattering imaging using photoacoustic measurements with one-wavelength illumination *J. Opt.* **16** 065301
[42] Xie Z, Wang L V and Zhang H F 2009 Optical fluence distribution study in tissue in dark-field confocal photoacoustic microscopy using a modified Monte Carlo convolution method *Appl. Opt.* **48** 3204–11
[43] Khokhlova T, Pelivanov I and Karabutov A 2008 Optoacoustic tomography utilizing focused transducers: the resolution study *Appl. Phys. Lett.* **92** 024105
[44] Lin S-P, Wang L, Jacques S L and Tittel F K 1997 Measurement of tissue optical properties by the use of oblique-incidence optical fiber reflectometry *Appl. Opt.* **36** 136–43
[45] Gao F, Feng X and Zheng Y 2014 Photoacoustic phasoscopy super-contrast imaging *Appl. Phys. Lett.* **104** 213701
[46] Di Ninni P, Bérubé-Lauzière Y, Mercatelli L, Sani E and Martelli F 2012 Fat emulsions as diffusive reference standards for tissue simulating phantoms? *Appl. Opt.* **51** 7176–82
[47] Perekatova V, Fiks I and Subochev P 2014 Image correction in optoacoustic microscopy. Numerical simulation *Radiophys. Quantum Electron.* **57** 67–79
[48] Roitner H, Haltmeier M, Nuster R, O'Leary D P, Berer T, Paltauf G, Grün H and Burgholzer P 2014 Deblurring algorithms accounting for the finite detector size in photoacoustic tomography *J. Biomed. Opt.* **19** 056011
[49] Jaeger M, Schüpbach S, Gertsch A, Kitz M and Frenz M 2007 Fourier reconstruction in optoacoustic imaging using truncated regularized inverse *k*-space interpolation *Inverse Problems* **23** S51
[50] Michailovich O V and Tannenbaum A 2006 Despeckling of medical ultrasound images *IEEE Trans. Ultrason. Ferroelectr. Freq. Control* **53** 64–78